Asociación Argentina
de Mecánica Computacional

Mecánica Computacional Vol XXVIII, págs. 3011-3035 (artículo completo)
Cristian García Bauza, Pablo Lotito, Lisandro Parente, Marcelo Vénere (Eds.)
Tandil, Argentina, 3-6 Noviembre 2009

FINITE ELEMENT MODELLING OF SHAPE METAL DEPOSITION

A. Anca[1], V. Fachinotti [1] and A. Cardona[1]

[1] *Centro Internacional de Métodos Computacionales en Ingeniería (CIMEC-INTEC), Universidad Nacional del Litoral - CONICET, Güemes 3450, CP 3000 Santa Fe, Argentina*

Keywords: Shape Metal Deposition, Welding Simulation, FEM, Solids Mechanics, Thermal, Stresses

Abstract. Shape Metal Deposition (SMD) is a novel process for rapid prototyping that employs Tungsten inert gas (TIG) welding. The state of the art can be enhanced through modelling and control. It is of industrial interest to develop systematized models to explain observed phenomena and to allow prediction of processing conditions for process planning and optimization. In this work, the thermal and mechanical finite element modelling of SMD are presented. The thermal problem is solved with linear tetrahedral finite elements taking into account the liquid/solid phase change phenomena. The mechanical problem is solved with tri-linear hexahedral elements using a mixed formulation. Special techniques to account for the added material were developed. A set of numerical tests were conducted to determine the heat source model parameters, with validation by compared to experimental in a Ti6Al4V thick plate were developed in order to validate the implemented formulations. Tests consist on TIG washing procedures (welding without wire feeding in order to preheat the plate) followed by welded beads. Finally the experimental results including temperatures and displacements are compared with those obtained with the FEM code.

1 INTRODUCTION

One of the traditional methods of complex metal parts manufacturing has been the casting process. Industry is currently developing manufacturing processes that tend to replace the traditional casting processes. Shape Metal Deposition (SMD) is one of the procedures to generate prototypes of metal parts, usually built with expensive materials, in the shortest time possible and with minimal post-machining. SMD manufactured parts have the ability to achieve better mechanical properties because of the more consistent solidification process during deposition (Clark et al., 2008). Currently, the aero-space industry is interested in developing this type of manufacturing processes.

SMD consists of depositing molten material on a path by using a welding equipment guided by a robotic arm. Process parameters that give rise to successfully manufactured pieces are determined by trial and error. This procedure is very costly and time consuming. It is useful to determine a priori the set of parameters that result in less piece-work distortion with less residual stresses and appropiate micro-structural properties.

Because of the constant improvement of the computing capacity, it is currently possible to make three dimensional models that reproduce the process by numerical simulation. The finite element method has proven to be a robust method for predicting the temperature field, strain and displacement in non-stationary and nonlinear problems with phase change in metals (Huespe et al., 2000; Fachinotti, 2001; Thomas and Parkman, 1997). The aim of this work is to generate a simulation tool that assists in the design and planning of the SMD manufacturing process.

Fusion welding is a process in which the substrate and the filler wire are heated locally over the melting point, obtaining in this way a localized coalescence of both parts. The analysis of welding processes involves several branches of Physics, and requires the coupling of different models to describe the behavior of a phenomenological system. Different physical phenomena occur during the welding process, involving the interaction of thermal, mechanical, electrical and metallurgical fields. The temperature field is a function of many welding parameters such as arc power, welding speed, welding sequences and environmental conditions (Nami et al., 2004). The current work is focused on three-dimensional study of thermal and mechanical processes during shape metal deposition. A multi-dimensional solidification problem in which solidification takes place over a temperature range (typical in steel alloys) is implemented using a discontinuous integration scheme (Fachinotti et al., 1999b) along the discontinuities that are involved in this kind of problem. A mathematical model was employed to represent the power density distribution of the external heat source.

A standard finite element formulation limited to the solid domain has been adopted for the mechanical analysis. A particular methodology is implemented to deal with the cyclical melting/solidifying mechanical elements and to handle the newly added material.

The coupled thermo-mechanical models used in this work were previously validated by Anca (2008) and are extended to simulate de SMD process.

An experimental test was developed which measurements were then compared with those obtained using the presented model.

Finally a multi-layered wall application example is presented.

2 THERMAL PROBLEM

In this section, a temperature-based finite element model to simulate unsteady conduction heat transfer problems in a 3D media undergoing mushy phase change is briefly described. A more detailed description can be read in Fachinotti et al. (1999a, 2001).

The analyzed domain is discretized using linear tetrahedral Galerkin finite elements. During phase change, a considerable amount of latent heat is released or absorbed, causing a strong non-linearity in the enthalpy function. In order to model correctly such phenomenon, we made a exact integration distinguishing between the different one-phase subregions over those finite elements embedded into the solidification front.

Since contributions from different phases are integrated separately the sharp variations of the material properties between phases are easily captured. This, so called, discontinuous integration avoids the regularization of the phenomenon, allowing the exact evaluation of the discrete non-linear governing equation, which is solved using a full Newton-Raphson scheme with line-search.

The scheme was validated by comparison with the exact solution of Özisik and Uzzell (1979) and the results can be found in Anca et al. (2004) and Anca (2008).

2.1 Problem definition

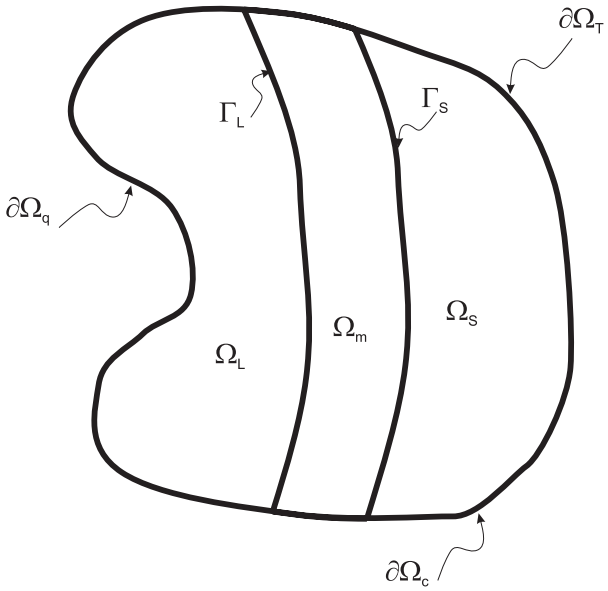

Figure 1: Thermal problem definition.

Under the assumptions of incompressibility, negligible viscosity and dissipation, linear dependence of the heat flux on temperature gradient (Fourier's law), and no melt flow during the solidification process, the energy balance for each subdomain Ω_i is governed by the classical energy balance equation

$$\rho\frac{\partial\mathcal{H}}{\partial t} - \nabla\cdot(\kappa\nabla T) = q \quad \forall(\boldsymbol{x},t)\in\Omega_i \tag{1}$$

where T denotes the temperature, $\mathcal{H}(T)$ the enthalpy (per unit volume), $\kappa=\kappa(T)$ the material thermal conductivity, assumed isotropic, and $q=q(\boldsymbol{x},t)$ is the welding volume heat input (to be defined later in Section 2.2 in the context of welding analysis). Equation (1) is supplemented by the following initial condition

$$T = T_0 \quad \forall\boldsymbol{x}\in\Omega_i, \quad t=t_0$$

and the boundary conditions on $\partial\Omega$:

$$T = \bar{T} \quad \text{at } \partial\Omega_T \tag{2}$$

$$-\kappa\nabla T \cdot \boldsymbol{n} = \bar{q} \quad \text{at } \partial\Omega_q \tag{3}$$

$$-\kappa\nabla T \cdot \boldsymbol{n} = h_{env}(T - T_{env}) \quad \text{at } \partial\Omega_c \tag{4}$$

being $\partial\Omega_T$, $\partial\Omega_q$ and $\partial\Omega_c$ non-overlapping portions of the body boundary $\partial\Omega$, with prescribed temperature, conductive and convective heat flux, respectively. In the above, $\bar{T}$ and $\bar{q}$ refer to imposed temperature and heat flux fields, and T_{env} is the temperature of the environment, whose film coefficient is h_{env}; $\boldsymbol{n}$ denotes the unit outward normal to $\partial\Omega$.

Further, the following continuity conditions must hold at the interface(s) Γ:

$$T = T_\Gamma \tag{5}$$

$$\langle \mathcal{H}u(\boldsymbol{\eta}) + \kappa\nabla T \cdot \boldsymbol{\eta} \rangle = 0 \tag{6}$$

where T_Γ is a constant value (equal to the melting temperature for isothermal solidification, and either the solidus or liquidus temperature otherwise), $\langle * \rangle$ denotes the jump of the quantity $(*)$ in crossing the interface Γ, which is moving with speed u in the direction given by the unit vector $\boldsymbol{\eta}$. Note that the second equation states the jump energy balance at the interface.

The detailed description of the thermal problem with phase change and no heat source was presented in our previous works (Anca et al., 2004; Anca, 2008; Fachinotti et al., 1999a). Now, let us focus in the introduction of a heat source model capable of reproducing welding arc sources.

2.2 Heat Source Modeling in Welding

The moving heat source is implemented as a typical transient formulation where the heat source moves along the part with time. In order to model the heat source the three-dimensional double ellipsoid proposed by Goldak et al. (1984) is studied (Figure 2). One characteristic of the double ellipsoid geometry is that it can be easily changed to model both the shallow penetration arc welding processes and the deeper penetration of laser and electron beam processes. The heat flux distribution is Gaussian along the longitudinal and transverse axes. The shape of the front half of the source is a quadrant of one ellipsoid source while the rear half shape is that of the quadrant of different ellipsoid. Four parameters define each ellipsoid. Physically, they correspond to the dimensions of the molten zone. Knowing the cross-section of the molten zone from experiments, the heat source parameters can be determined. As a first approximation, Goldak et al. (1984) assumed that it is reasonable to take the distance in front of the source equal to one half of the weld width and the distance behind the source equal to twice the weld width.

It is convenient to introduce a coordinate ξ, fixed on the heat source and moving with it. The moving reference frame on the heat source is related to the coordinate fixed on the work piece by:

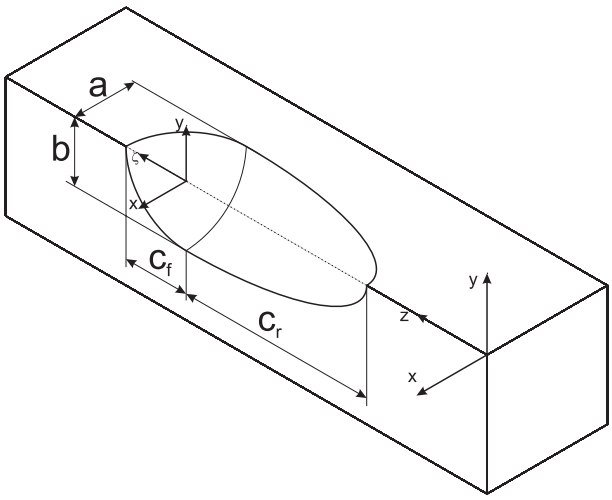

Figure 2: Goldak double ellipsoid heat source.

$$\xi = z - v(t - \tau) \tag{7}$$

where v is the welding speed and τ is the time lag necessary to define the position of the heat source at time $t = 0$. The weighting fractions associated with the front and rear ellipsoids are denoted by f_f and f_r, respectively, and these fractions are specified to satisfy $f_f + f_r = 2$. Let us denote q the power density in W/m^3 within the ellipsoid, and let a , b and c denote the semi-axes of the ellipsoid parallel to the x, y, ξ axes. Then, the power density distribution inside the front quadrant, is specified by

$$q(x, y, \xi) = (\frac{6\sqrt{3} f_f Q}{abc_f \pi \sqrt{\pi}}) \exp(-3\frac{x^2}{a^2}) \exp(-3\frac{y^2}{b^2}) \exp(-3\frac{\xi^2}{c_f^2}) \tag{8}$$

and in the rear quadrant it is specified by

$$q(x, y, \xi) = (\frac{6\sqrt{3} f_f Q}{abc_r \pi \sqrt{\pi}}) \exp(-3\frac{x^2}{a^2}) \exp(-3\frac{y^2}{b^2}) \exp(-3\frac{\xi^2}{c_r^2}) \tag{9}$$

In these equations, Q is the heat available at the source. For an electric arc the heat available is

$$Q = \eta V I \tag{10}$$

where η is the heat source efficiency, V is the arc voltage, and I is the arc current. The parameters a, b, c_f and c_r are independent, and can take different values to properly model the weld arc.

The spatial distribution of heat is calculated from equations (8) and (9) and is applied as a volumetric heat generation.

The implemented moving heat source model was verified by comparing with the experimental test of Christensen et al. (1965) (Anca, 2008) and with an analytical solution for the transient temperature field of a semi-infinite body subjected to 3-D power density moving heat source presented in Fachinotti et al. (2009).

Remark:

- To ensure that the integral over the elements of the power density distribution equals to the total prescribed power, a global scaling factor is applied to the heat flow of those nodes that belong to the double ellipsoid region.

3 MECHANICAL PROBLEM

During a thermal welding process, the weld site and immediate surrounding area experience different rates of heating/cooling and thus expansion/contraction. This effect leads to considerable thermal strains. Due to the heat application localized nature, the expansion due to these strains is constrained by the cool material away from the site of the applied heat. It should be noted that the weld pool itself is not modelled in the mechanical analysis. This is only a soft region serving for heat input to the thermomechanical model. In this sense, the existence of a cut-off or *Zero Strength Temperature* ZST was assumed. The ZST is defined as the minimum temperature amongst those at which strength is zero (Nakagawa et al., 1995). This is also the temperature above which no further changes in material properties are accounted for in the mechanical analysis.

In the numerical model we have implemented, the plastic material is considered to be rate independent with an associative J_2 von Mises law and isotropic hardening (Simo and Hughes, 1998). We used rate-independent plasticity at high temperatures because of the involved time scales (Lindgren, 2001): in the weld thermal cycle the material has a high temperature during a relatively short time, and therefore the accumulated rate-dependent plasticity may be neglected. Inertial effects are ignored in the momentum balance equations, according to the assumption of null acceleration within the solid.

3.1 Melting-Solidifying Behavior

It is recognized that finite element techniques, with standard constitutive material modelling, yield good solutions in thermal stress analysis, even when the solid is subjected to temperatures near the solidification ones (Thomas and Parkman, 1997; Fachinotti and Cardona, 2003). However, there are particular aspects in the formulation for melting/solidifying problems that need to be carefully considered.

Three different configurations for every material point and its neighborhood (Figure 3) are considered for the mechanical simulation of this process:

i) the reference configuration (B), in which the particle label is assigned;

ii) the (intermediate) natural configuration (B^0) which corresponds to that state where the material point solidified just below the zero strength temperature (ZST), and started to develop mechanical strength;

iii) the current configuration (B^t).

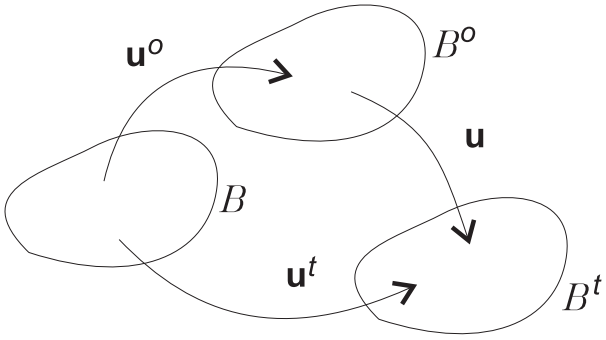

Figure 3: Reference (B), natural (B^0) and current (B^t) body configurations in the melting/solidification problem.

Note that since the solidification time instant is not the same one for all points in the domain of analysis, each material point has its own (intermediate) natural configuration.

Let us define $\boldsymbol{u}^o$ as the displacement from the reference to the natural configuration, $\boldsymbol{u}^t$ the displacement from the reference to the current configuration and $\boldsymbol{u}$ the displacement from the natural to the current configuration. Then, we can write:

$$\boldsymbol{u}^t = \boldsymbol{u} + \boldsymbol{u}^o \tag{11}$$

Usually, when a finite element procedure is used, the mesh is defined in the reference configuration (the set of points at time $t = 0$) as depicted schematically in Figure 4.

Let us consider that $\boldsymbol{X}$ and $\boldsymbol{x}^o$ are coordinate systems in the reference and natural configurations, respectively. As a consequence of the assumption of small deformations introduced to describe motion, and by assuming the existence of the intermediate deformation gradient in the neighborhood of every point, we can approximate : $\nabla_{\boldsymbol{X}} \boldsymbol{x}^o \approx \mathbb{I}$. The same assumption allows us to evaluate the strain $\boldsymbol{\varepsilon} = \nabla^{sym}_{\boldsymbol{x}^o} \boldsymbol{u}$, related to the motion from the natural to the final configurations, by the following approximation:

$$\boldsymbol{\varepsilon} = \nabla^{sym}_{\boldsymbol{x}^o} \boldsymbol{u} \approx \nabla^{sym}_{\boldsymbol{X}} \boldsymbol{u} \tag{12}$$

By taking gradients in equation (11) and using the assumptions stated above, we can verify the validity of the additive decomposition of strains:

$$\boldsymbol{\varepsilon}^t = \boldsymbol{\varepsilon} + \boldsymbol{\varepsilon}^o \tag{13}$$

where $\boldsymbol{\varepsilon}^t = \nabla^{sym}_{\boldsymbol{X}} \boldsymbol{u}^t$ is the strain tensor at the actual configuration (time t) with respect to the reference configuration, and $\boldsymbol{\varepsilon}^o = \nabla^{sym}_{\boldsymbol{X}} \boldsymbol{u}^o$ is the strain at the natural configuration with respect to the reference one.

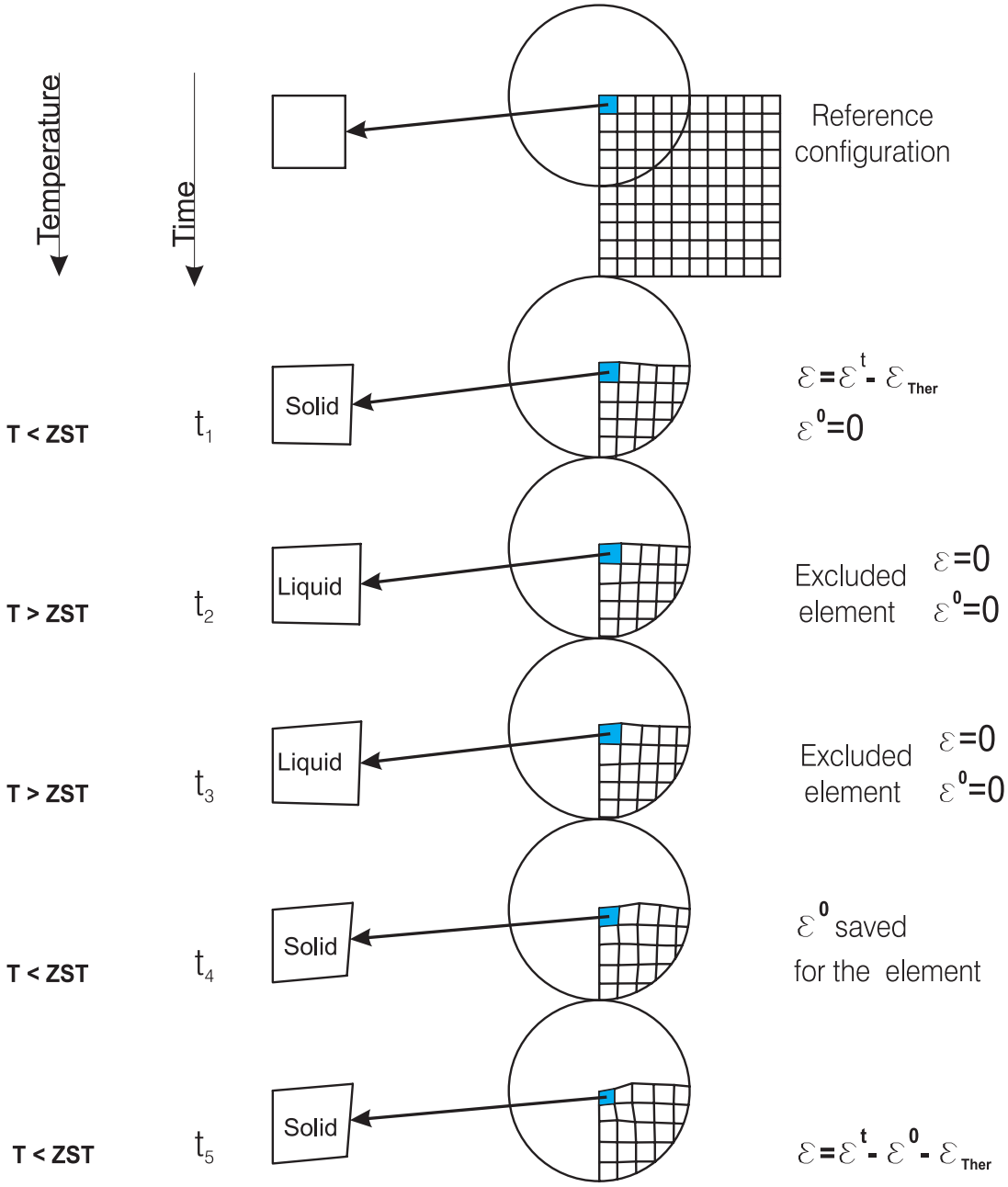

Figure 4: Evolution of d.o.f.s and strains in melting/solidification problems.

For a correct representation of the steel constitutive behavior in the zone of interest, it is mandatory to account for the strong dependence of the material parameters on temperature.

Remarks:

- The strain ε^o is computed the first time that all nodal temperatures of the considered element fall below the zero strength temperature (ZST), and is stored at the finite element Gauss point as an additional tensorial internal variable. In this work ZST is set equal to the metal solidus temperature.

- In this model, the solid phase domain changes with time. This fact introduces some difficulties concerning the mesh definition for the FE analysis. The procedure we have imple-

mented consists in defining a fixed mesh that describes the complete domain, including the liquid and mushy zones. Nodes in the liquid and mushy zones are initially fixed. In subsequent time steps, when the nodal temperatures fall below the ZST, nodal d.o.f.'s are freed and the stiffness contribution of the solidified zone is taken into consideration (see Figure 4).

- The described numerical model does not predict the real displacement field of the zones that have melted, because the displacement field of the natural configuration is not recorded.
- The technique of subtraction of the strain term ε^o from the total strain ε^t must be emphasized for its simplicity and accuracy. The technique is validated in the examples by comparison with results obtained by using the semi-analytical formulation of Weiner and Boley (1963). Note also that this approach is less expensive than those used by other authors, which are based on recording the flow strain for liquid elements (Abid and Siddique, 2005; Yaghi and Becker, 2004).
- All elements internal variables, included the ε^o strain, are set to zero as soon as the element temperature rises above ZST.
- Mechanical elements have a special treatment during the liquid/solid and solid/liquid phase changes: while the temperature is above the ZST, the corresponding elemental d.o.f.'s are not included in the system of equations for the unknowns of the mechanical problem. This methodology incorporates an advantage compared to other techniques found in literature (e.g. assigning a very low stiffness to the elements that are in liquid/mushy phases brings poor conditioning of the algebraic equation system to be solved).

To avoid restructuring the stiffness matrix at each time step, liquid mechanical d.o.f.'s are uncoupled from the rest by zeroing the corresponding rows and columns, and putting a non-zero term in the diagonal entry of the stiffness matrix. Also, the corresponding position in the residue is zeroed.

3.2 Finite element implementation

Incompressible material behavior may lead to some difficulties in numerical simulation, such as volumetric locking, inaccuracy of solution, checkerboard pattern of stress distributions, or occasionally, divergence. Mixed $\boldsymbol{u}$-p elements, with both displacements and hydrostatic pressure as primary unknown variables, are used to overcome these problems.

By ignoring inertial effects, the momentum balance equation can be written as:

$$\nabla \cdot \boldsymbol{\sigma} + \rho \boldsymbol{b} = 0 \quad \text{in} \Omega, \tag{14}$$

subjected to the following boundary conditions

$$\boldsymbol{u} = \bar{\boldsymbol{u}} \quad \text{on} \partial\Omega_u \tag{15}$$

$$\boldsymbol{\sigma} \cdot \boldsymbol{n} = \bar{\boldsymbol{t}} \quad \text{on} \partial\Omega_t, \tag{16}$$

A mixed FEM displacement and pressure formulation is used to solve the momentum balance equation.

Since the material is only nearly incompressible and the pressure variables are considered at the elemental level only, then we can statically condense out the pressure terms and express the element matrices in terms of displacements only.

As pointed out by Cifuentes and Kalbag (1992) and Benzley et al. (1995), hexahedral elements are superior to linear tetrahedral elements, and also better than quadratic tetrahedron elements when plastic deformation occurs. Therefore, we used $q1 - p0$ hexahedral elements in our tests.

The discrete equilibrium equations are solved by using a standard Newton-Raphson method. The Jacobian matrix corresponds to that obtained from an equivalent purely Lagrangian elasto-plastic quasi-static incremental problem (see for instance Simo et al. Simo and Hughes (1998)).

4 THERMAL-MECHANICAL PROBLEM

Due to the weak nature of mechanical to thermal field coupling, at each time step, the solution of the non-linear transient problem is divided in two parts. First, a thermal analysis is performed to predict the temperature history of the whole domain, and then the temperature field is applied as input for the subsequent mechanical analysis, in a staggered approach.

As pointed out in Section 3 hexahedral finite elements are used to solve the mechanical problem. On the other hand, the thermal problem is solved using tetrahedral elements. In order to share the same nodes in both problems, first a mesh of hexahedra for the mechanical model is generated. Then by splitting each hexahedron in six tetrahedra, the thermal finite element mesh is obtained.

5 FILLER MATERIAL MODELING

The process of filler metal addition is described in this section.

An activating element technique to model the added material during the deposition has been used. A unique finite element mesh, both for substrate and for each metal layer to be deposited in each pass, is generated. Each finite element is associated to an activation parameter. The activation parameter is an element property and it is assigned at the time of built the mesh. During execution of an analysis , and before starting a new time step, the elemental activation parameter is compared with the current analysis time for all elements in the mesh. The elements whose activation parameter is greater than or equal to the current calculation time will be taken into account when making the assembly of the system of equations. While an element is in deactivated mode, its degrees of freedom are not included in the system of equations to be solved for the present time. When thermal elements are activated, they enter with an initial temperature equal to the metal liquidus temperature. Mechanical elements are specially treated in order to account for the cyclic melting and solidification behaviour as described in Section 3.1. The element mechanical historical variables enter with zero value and in liquid state. Therefore, the mechanical degree of freedom are not taken into account until its temperature is less than the ZST set for the calculation.

The thermal domain is composed of all substrate elements and the elements that have been activated during the analysis. The Figure 5 shows, for a given time step, the elements that have been taken into account in calculating temperatures. In black can be distinguished elements that have been recently incorporated for these time step. On the other hand, the domain for the mechanical problem is represented for the same time step in Figure 6. In this case only shows the items in which the temperature at all nodes is less than the ZST. In black is shown the group of elements that have been added for this time step and are not part of the calculation domain.

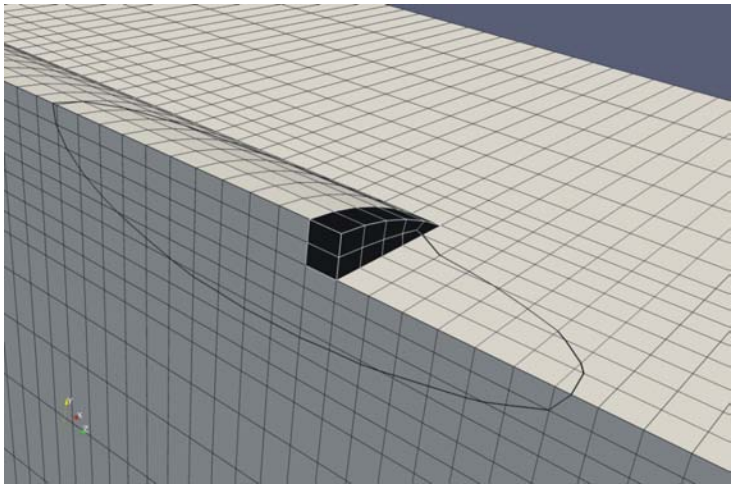

Figure 5: The thermal domain of analysis, showing in black, the newly added material and the ZST isotherm.

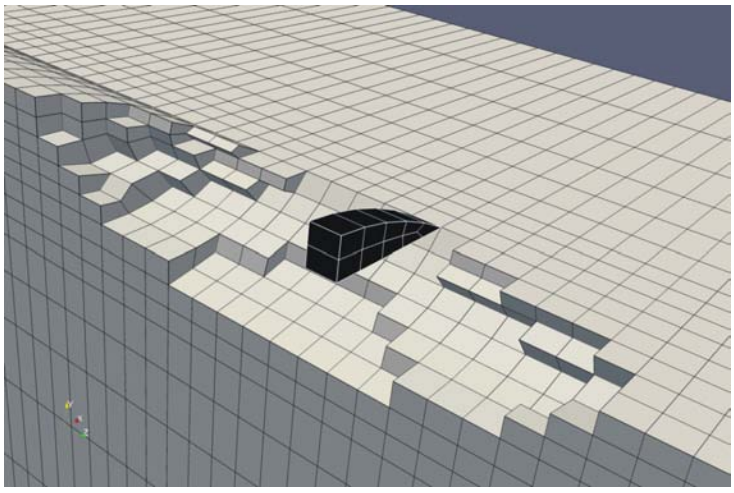

Figure 6: The mechanical domain of analysis. In black, the newly added material.

Remark:

- In case a set of newly added elements lie outside the ZST isotherm they are forced to be trated as liquid element and they are excluded of the mechanical analysis domain.

6 APPLICATION EXAMPLE

6.1 Experimental test

In the present research an experimental TIG single layer weld deposition bead on a flat plate substrate of Ti-Alloy was performed. Prior to the actual bead deposition a TIG-wash procedure is performed consisting in preheating the deposition site with the torch without wire feeding. The experiment was conducted in order validate the present code and to identify the welding heat source parameters. The base plate and wire are made of Ti-6Al-4V. The heat power, the travel speed and the wire feed rate are summarized in Table 1.

Arc Parameter	Symbol	Value
Current- TIG-wash	I	160 A
Current- actual bead	I	180 A
Voltage	U	12 V
Speed	v	5 mm/s
Wire Feed Rate	WFR	2.3 mm/min

Table 1: Arc parameters.

During the metal deposition, the plate was held in place by a fixture with two contact points on each side, which can be seen in Figure 7.

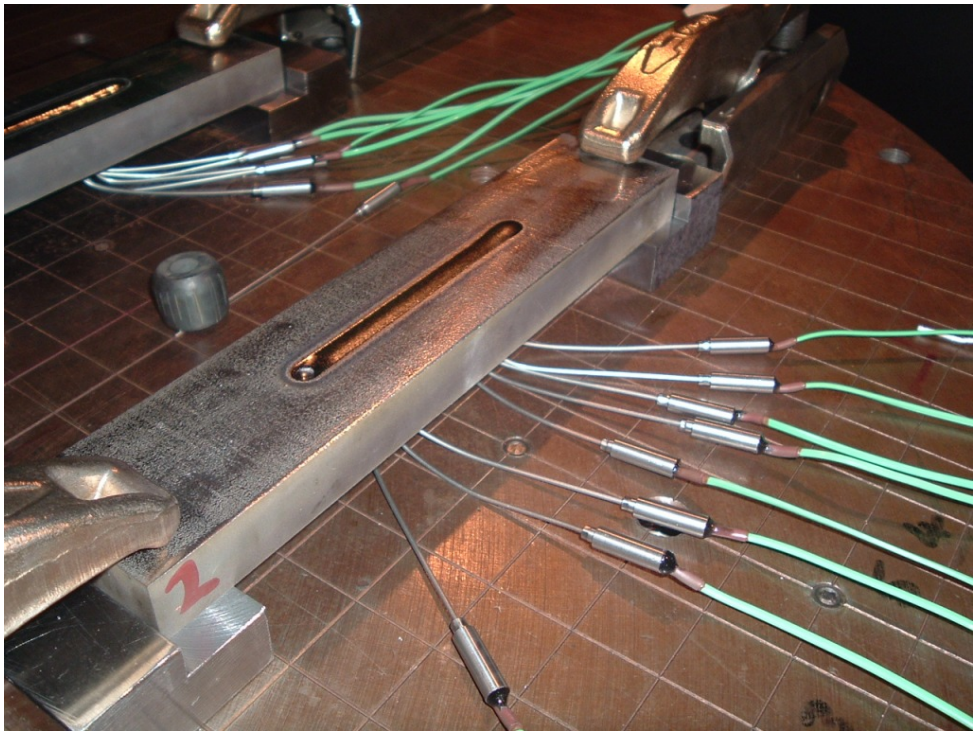

Figure 7: Experimental set up

Eight thermocouples were welded on the plate, positioned as shown in Figure 7.

The entire process was performed within a chamber. A protective atmosphere was maintained by injecting Argon into the chamber.

After the TIG-wash procedure, a weld bead was built in the center of the plate. The final bead has $9.23\ mm$ wide by $1.28\ mm$ height and $100\ mm$ long (Figure 8).

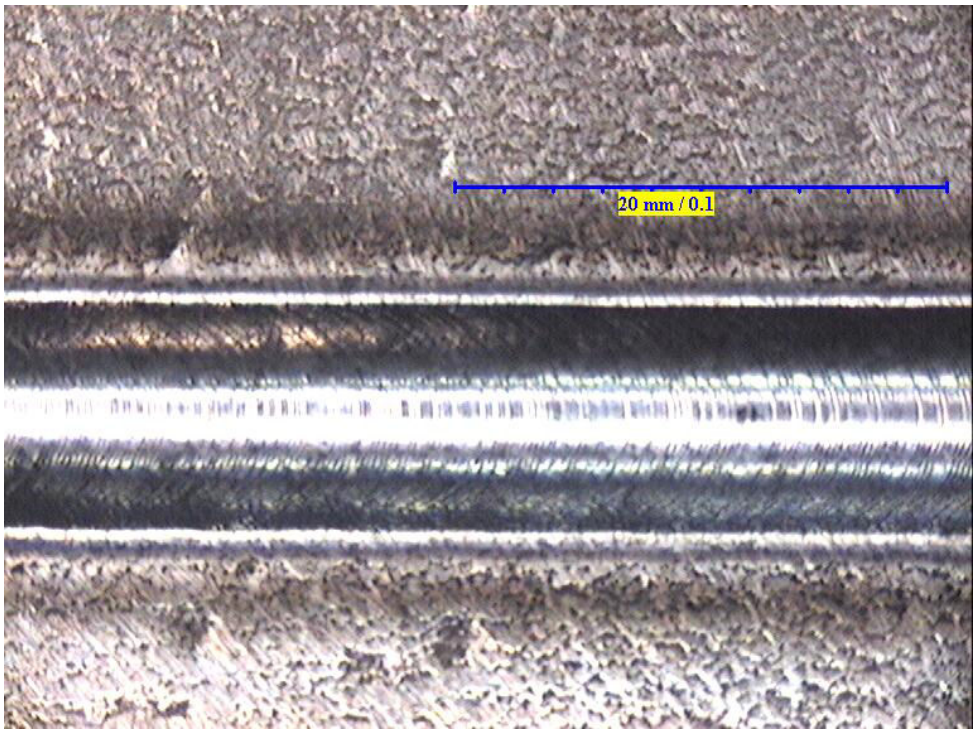

Figure 8: Final welding bead the surface

6.2 FEM Solution

In this example a heat source moves at constant speed and along a straight line over the welded plate. A 3-dimensional symmetrical model was used to estimate temperature, displacement and the residual stresses using the finite element method. The plane of symmetry is defined along the centerline of the weld path and perpendicular to the plate top surface.

The sample dimensions are shown in Figure 9. The x, y and z axes represent the width, thickness and length of the plate, respectively. The coordinate $y = 0$ corresponds to the top surface of the sample and $x = 0$ corresponds to the symmetry plane. The symmetric mesh model employs 28000 eight-node mechanical hexahedral elements with 33383 nodes and 140000 thermal tetrahedrons shearing nodes. The heat affected zone (HAZ) was refined locally and was coarsened gradually farther along the transversal and vertical direction as show in Figure 10.

A thermal-perfect-elastoplastic model is used in the analysis. The mechanical boundary conditions were $u_x(0,0,0) = 0; u_y(0,0,0) = 0; u_z(0,0,0) = 0$ and $u_x(0,0,0.25) = 0; u_y(0,0,0.25) = 0$ together with the symmetry condition at $x = 0$.

The constant material properties are summarized in table 2

The material thermo-mechanical properties dependent on temperature are shown in Figure 11 and 12.

Heat transfer in all surfaces of the plate was assumed. The convection-radiation coefficient h is variable with temperature as shown in Figure 13.

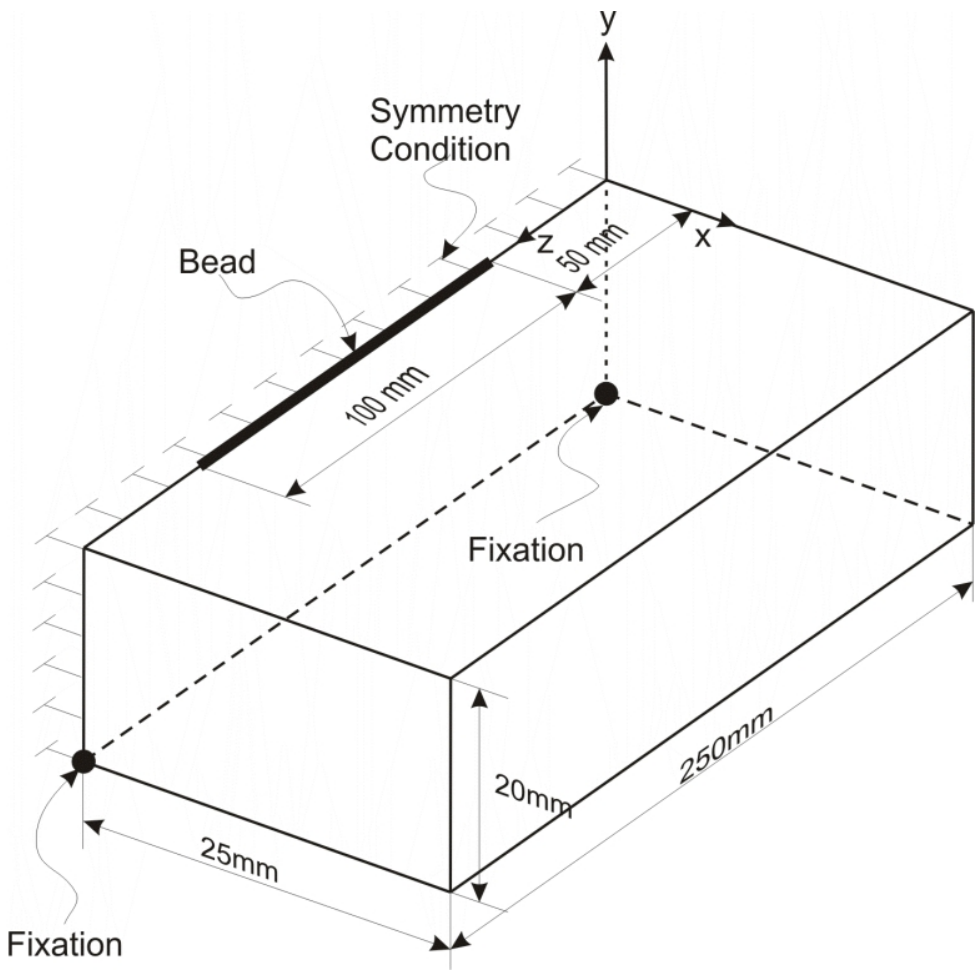

Figure 9: Plate dimensions and mechanical boundary conditions.

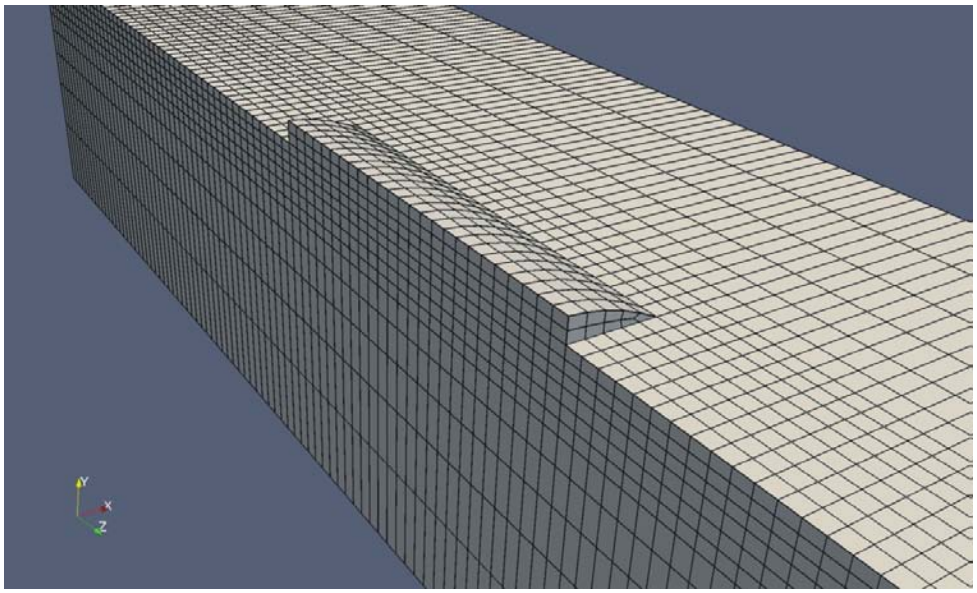

Figure 10: Finite Element Mesh.

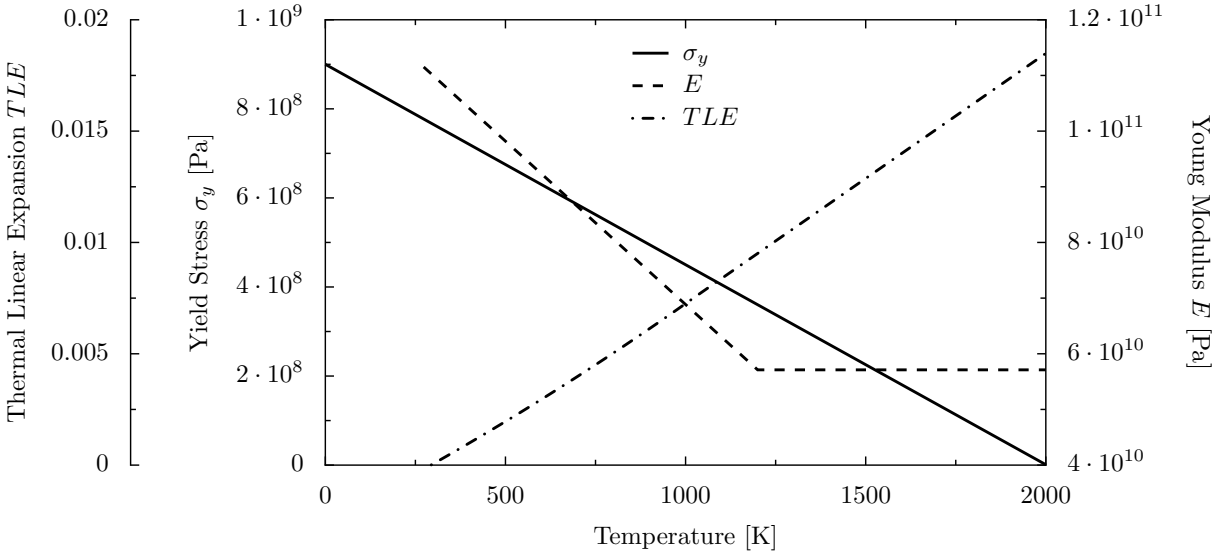

Figure 11: Mechanical properties as function of temperature

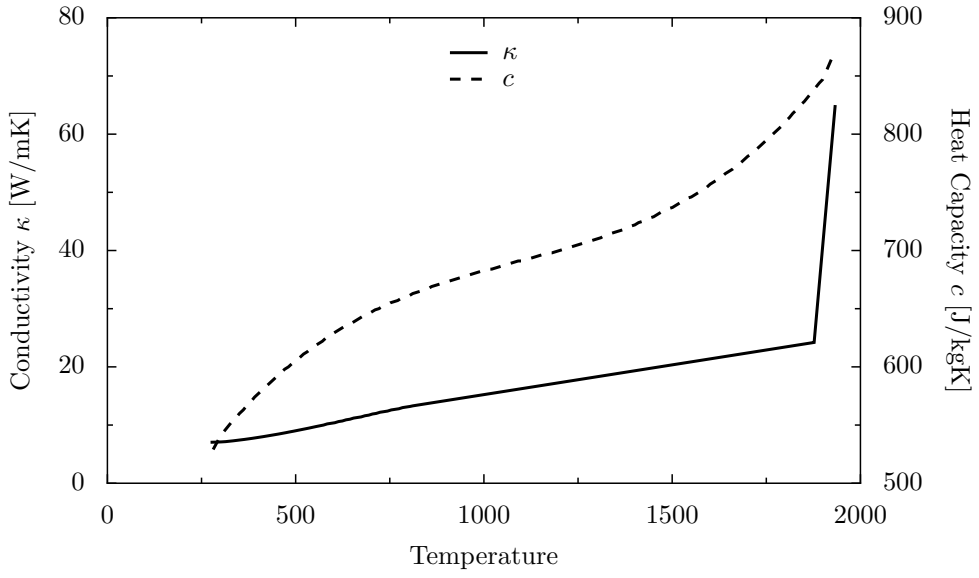

Figure 12: Thermal properties as function of temperature.

Parameter	Symbol	Value	Unit
Density	ρ	4430	$[kg/m^3]$
Latent Heat	$\mathcal{L}$	292600	$[J/kg]$
Solidus temp.	T_s	1877	$[K]$
Liquidus temp.	T_l	1933	$[K]$
Initial temp.	T_i	299	$[K]$
Zero Strength Temp.	ZST	1877	$[K]$
Poisson ratio	μ	0.34	

Table 2: *Material and problem data for the validation problem*

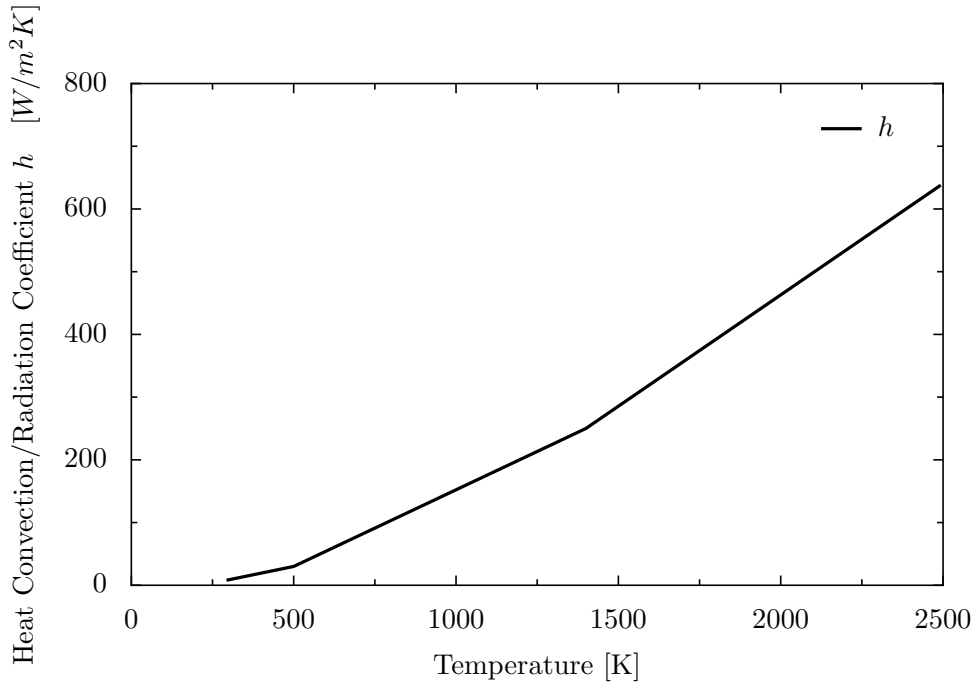

Figure 13: Hear covection/radiation coefficient as function of temperature.

Experimentally measured temperatures are used to calibrate the heat source parameters and the results are presented in Table 3.

6.2.1 Moving heat source

The double-ellipsoid heat source model as described in 2.2 was adopted to calculate volumetric heat flux distributions as heat input. The welding torch position along z and the total power used in the current analysis are ploted in Figures 14 as a function of time.

6.2.2 Simulation results

The time stepping has a minimum time step of 0.15 s during tg-wash and welding. The complete analysis has taken about 25 hs of CPU, on a 8 x Intel(R) Xeon(R) 2.66GHz processor with 32 GB of memory.

The acquired data from the thermocouples were used to calibrate the parameters of the heat source and they are shown together with the simulated temperatures in Figure 15 and 16. The sample points are for TC3 $(0, 0.0155, 0.080)$ and for TC5 $(0.010, 0.0165, 0.080)$.

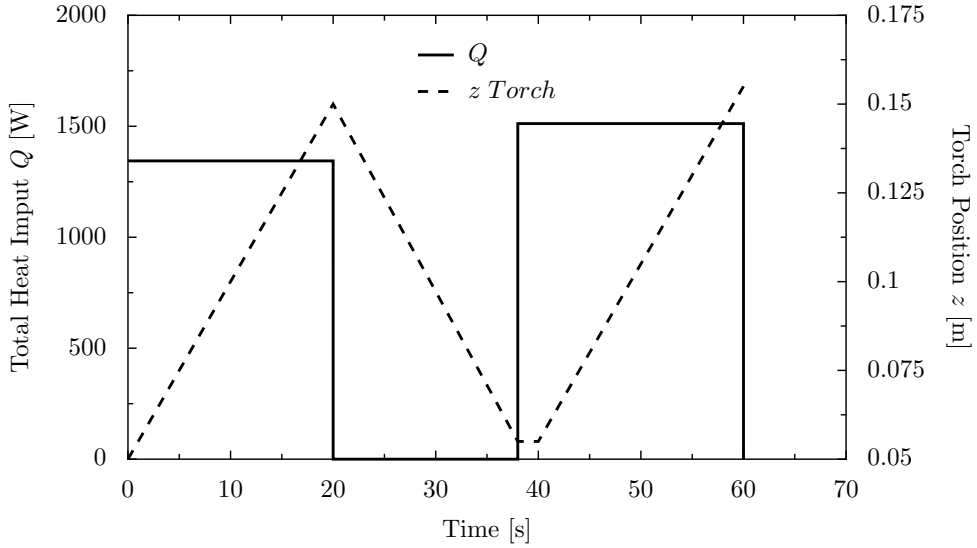

Figure 14: Total heat input and torch position as function of time.

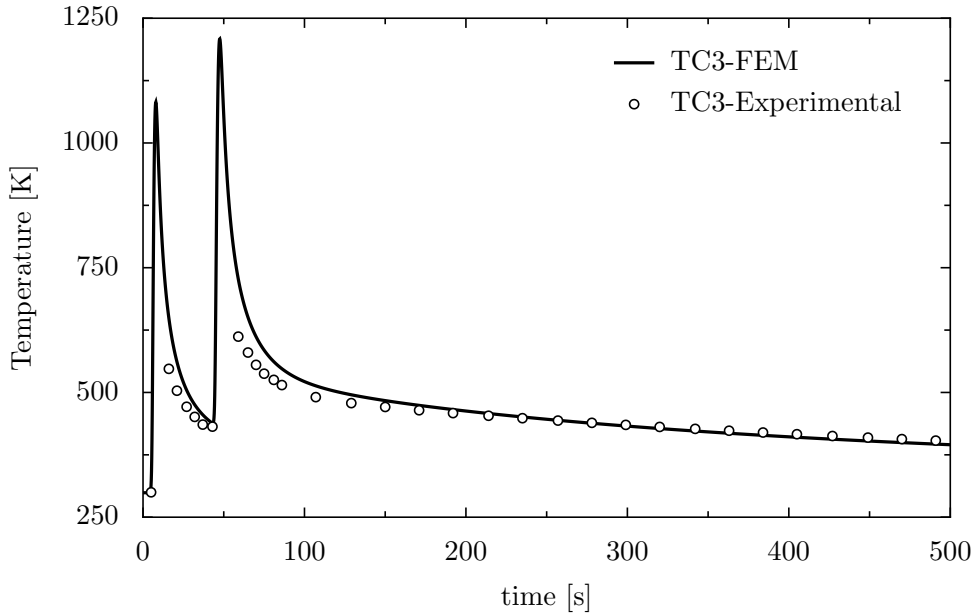

Figure 15: Comparison of predicted and measured temperature at point $(0, 0.0155, 0.080)$

.

Goldak Parameter	Value
a	5 mm
b	2 mm
c_f	5 mm
c_r	1.84 mm
f_f	$2\frac{c_f}{c_f+c_r}$
f_r	$2.0 - f_f$
Efficiency η	0.7

Table 3: Goldak parameters.

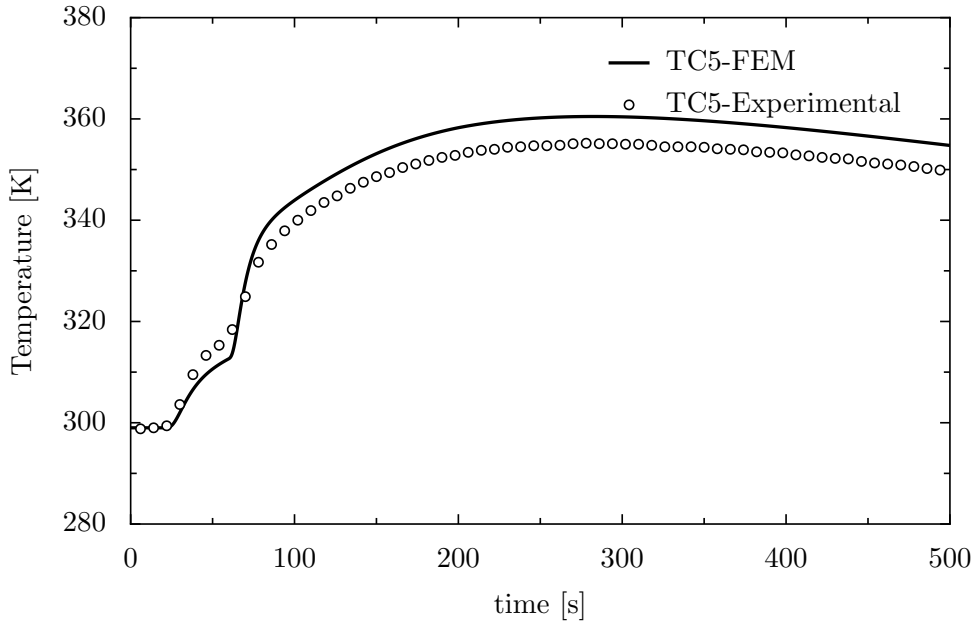

Figure 16: Comparison of predicted and measured temperature at point $(0.010, 0.0165, 0.080)$

.

Each temperature peak in Figure 15 represents the model response as the heat source passes the sample points. The rapidly decreasing temperature is caused mainly by conduction to the surrounding material.

Figures 17 to 18 show the simulated temperature field distribution for three different times, $t = 15s$ TIG-wash without filler material and $t = 55s$ the first pass. At the end of the simulation time ($t = 500s$) the work-piece states at $400\ K$. The white line in the Figures represents the ZST isothem, in the present analysis set equal to the solidus temperature and can be interpreted as the weld pool.

The calculated longitudinal σ_z transient stress field during welding and after cooling are shown in Figures 19, 20 and 21.

The the longitudinal σ_z stress map shows that a compressive stress is formed in front of the fusion zone, whereas a tensile stress is appearing at the back of it, mainly due to the thermal expansion effects.

The final $y - direction$ experimental displacement and computational model are compared in Figure 25.A quantitative distortion measure can be made by means of flatness of the top face. The experimental measured flatness of $0.7\ mm$ is compared with the calculated by simulation. The very good agreement between the FEM and experimental measurements gives confidence

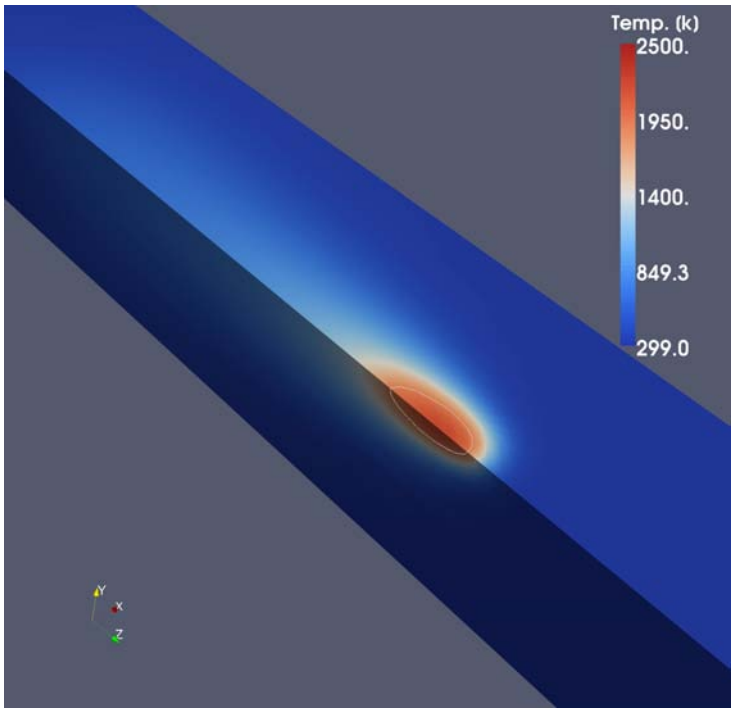

Figure 17: Fusion Zone Temperature field $[K]$ at time $t = 15s$.

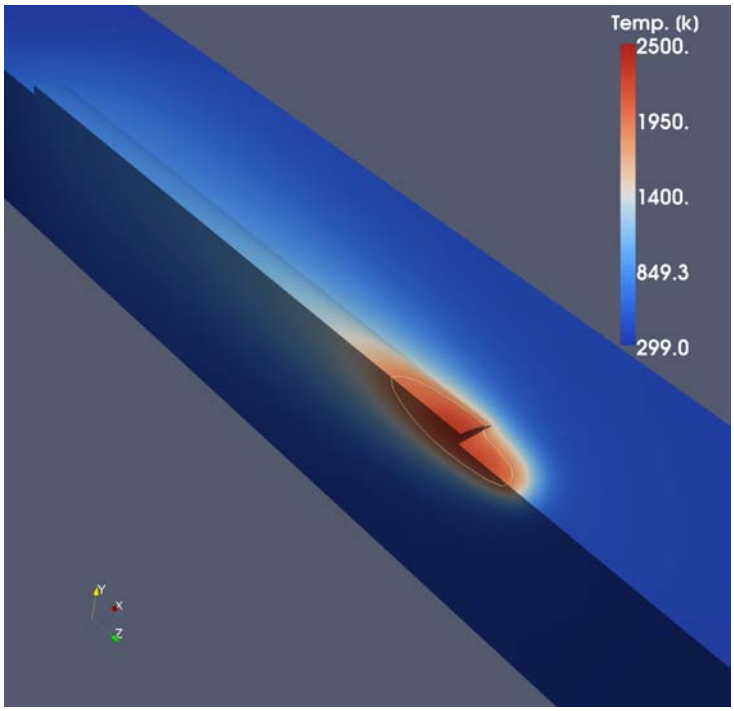

Figure 18: Fusion Zone Temperature field $[K]$ at time $t = 55s$.

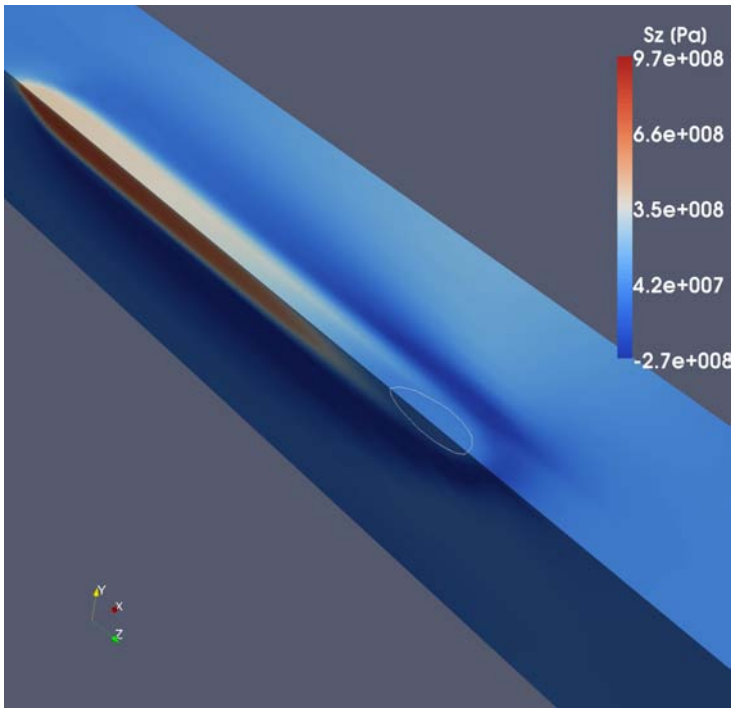

Figure 19: Longitudinal stress distribution at $t = 15s$

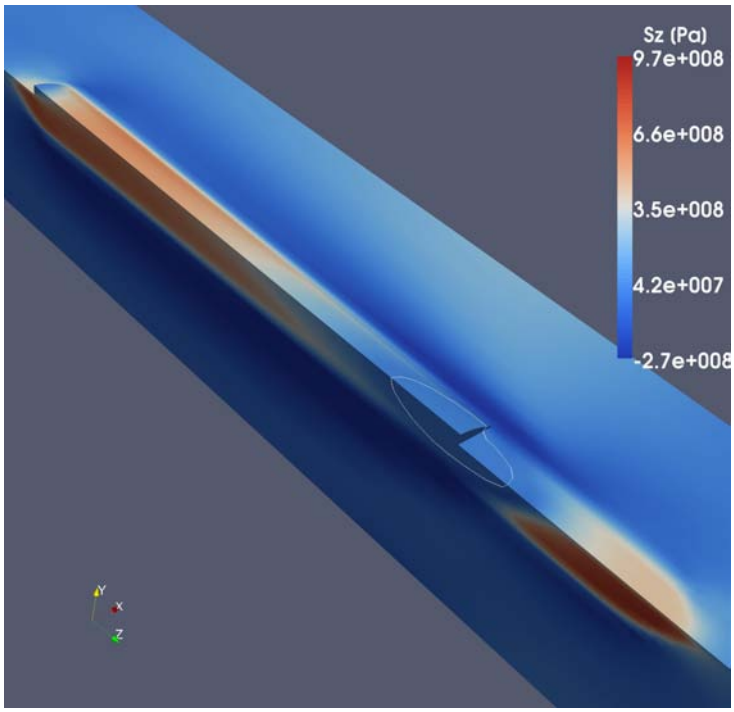

Figure 20: Longitudinal stress distribution at $t = 55s$

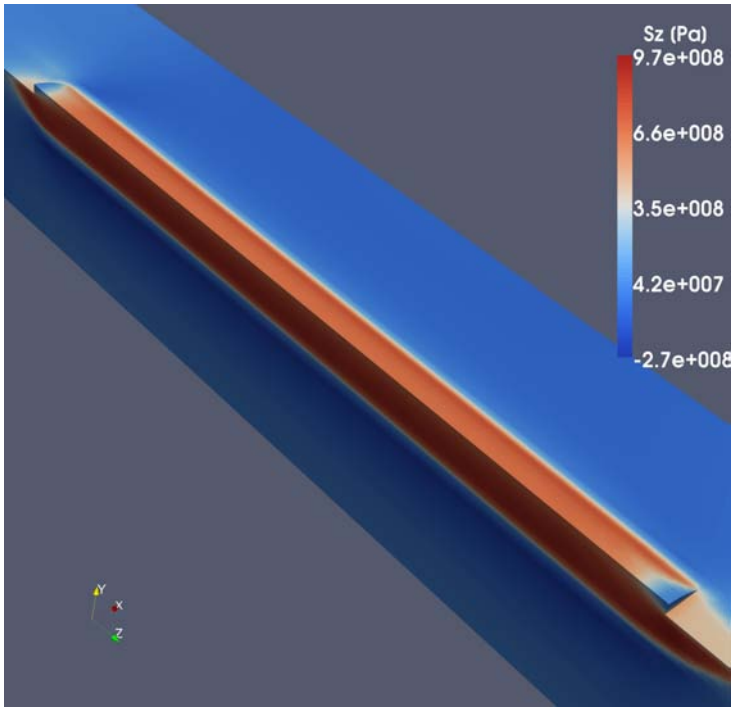

Figure 21: Final residual longitudinal stress distribution.

in developed finite element model.

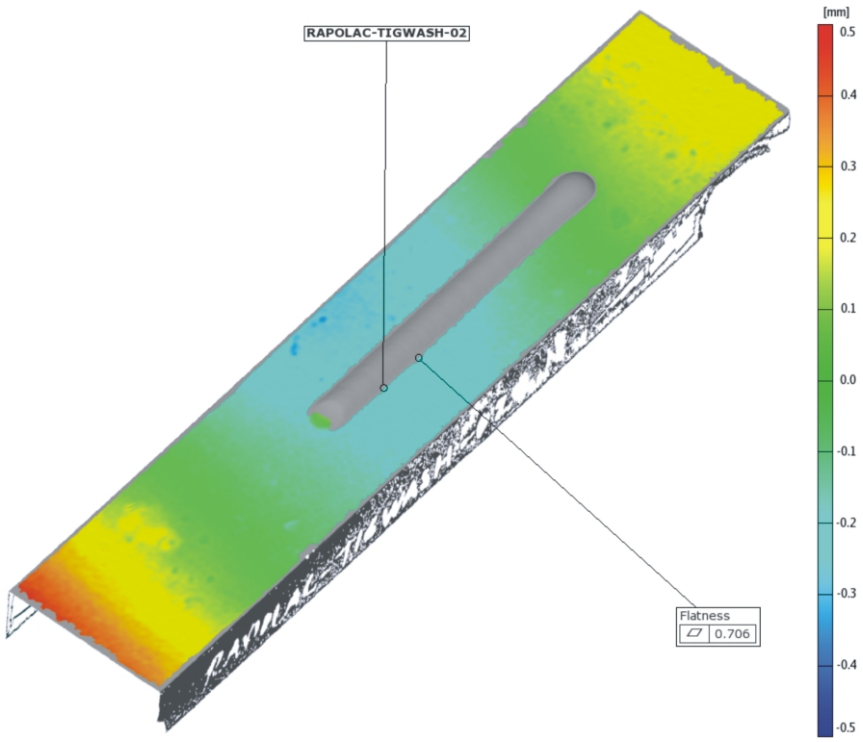

Figure 22: Experimenltal y displacement measurement.

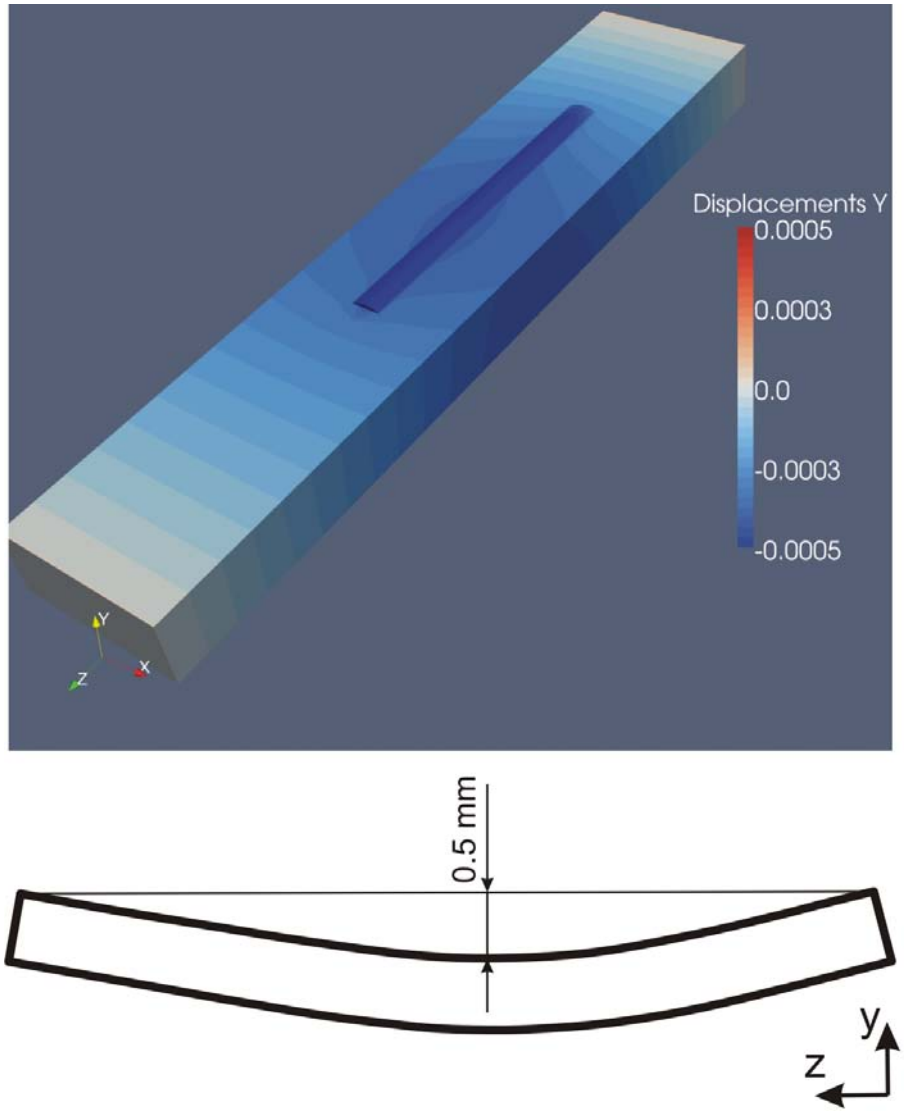

Figure 23: Computational out-of-plane displacement.

6.3 Multi Layer Deposition

In this section we present the simulation of the titanium wall construction by SMD. For this example we used the same geometry, material properties and process parameters in the previous example. The only difference lies in the number of layers that are deposited to form the wall.

The images sequence on Figures 24 and 25 shows the filler material that has been contributed for each layer in four time instants. Figure 26 and 27 shows the longitudinal stresses that are developed for the same time instants.

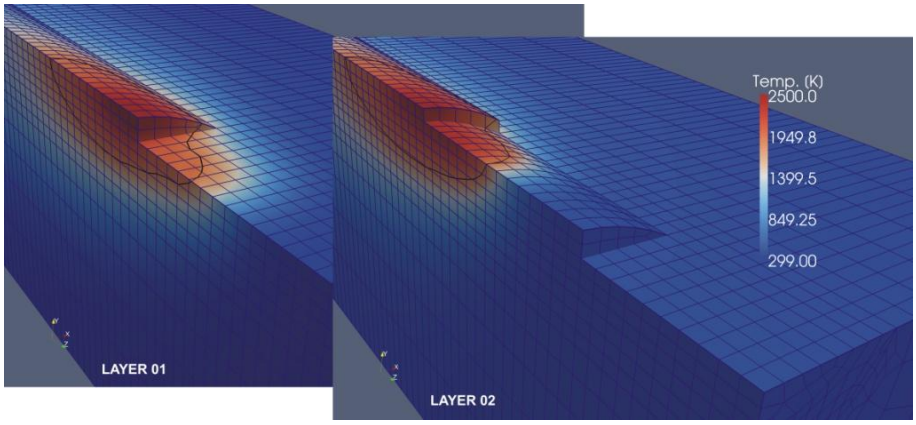

Figure 24: Temperature field and deposition of leyers 1 and 2.

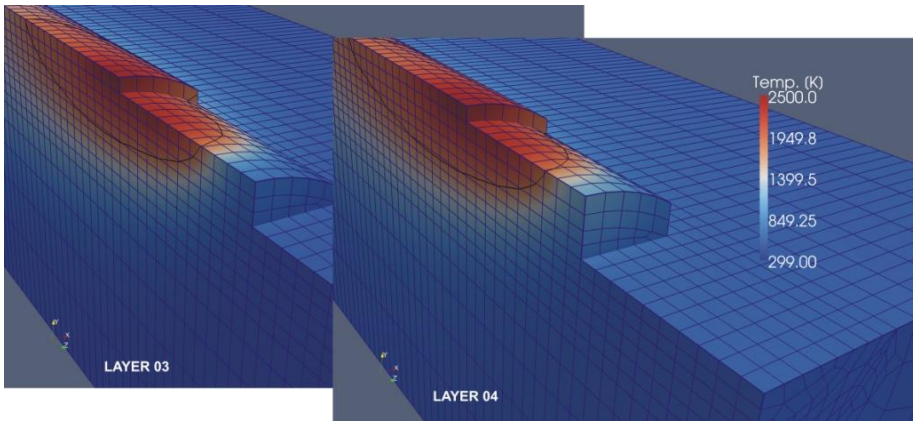

Figure 25: Temperature field and deposition of leyers 3 and 4.

7 CONCLUSIONS

In this paper we have presented a methodology to resolve by FEM the problem in order to modeling the temperature field, strains and stresses that occur during the manufacturing process of parts by SMD. It has been used a staggered resolution scheme. First the thermal model with phase change liquid / solid and external heat source is solved. Then with the temperature field as parameter, the domain of analysis to solve a mechanical problem on small deformations using a von Mises material model with isotropic hardening is determined. It has developed a special technique for the treatment of mechanical elements which are cyclically melt and solidify. The filler material used to create the piece by SMD is treated by a inclusion/exclusion of the degree of freedom in the system of equations for both the thermal and mechanical problem. The combination of both techniques has proved to be robust and has solved the bad conditioning problem, which is produced using fictitious rigidities associated with the inactive elements. We have developed an experimental test to validate the proposed models. The experimental results show acceptable agreement with those obtained by numerical simulation.

REFERENCES

Abid M. and Siddique M. Numerical simulation to study the effect of tack welds and root gap on welding deformations and residual stresses of a pipe-flange joint. *International Journal of Pressure Vessels and Piping*, 82:860–871, 2005.

Anca A. *Computer simulation of steel thermomechanical processes at high temperatures*. Ph.D. thesis, Universidad Nacional del Litoral (FICH/INTEC/CONICET, 2008.

Anca A., Cardona A., and Risso J. 3d thermo-mechanical simulation of welding processes. In G. Buscaglia, E. Dari, and O. Zamonsky, editors, *Mecánica Computacional, XIV Congreso de Métodos Numéricos y sus Aplicaciones (Enief 2004)*, volume XXIII, pages 2301–2318. 2004.

Benzley S., Perry E., Merkely K., Clark B., and Sjaardama G. A comparison of all hexagonal and all tetrahedral finite element meshes for elastic and elasto-plastic analysis. *Proc. 14th Ann. Int. Meshing Roundtable, Albuquerque, USA*, 1995.

Christensen N., Davies V.d.L., and Gjermundsen K. Distribution of temperatures in arc welding. *British Welding Journal*, 12:54–75, 1965.

Cifuentes A. and Kalbag A. A performance study of tetrahedral and hexahedral elements in 3-d finite element structural analysis. *Fin. Elem. Anal*, 12:313–318, 1992.

Clark D., Bache M., and Whittaker M. Shaped metal deposition of a nickel alloy for aero engine applications. *Journal of Materials Processing Technology*, 203(1-3):439 – 448, 2008. ISSN 0924-0136. doi:DOI:10.1016/j.jmatprotec.2007.10.051.

Fachinotti V., Anca A., and Cardona A. Analytical solutions of the thermal field induced by moving double-ellipsoidal and double-elliptical heat sources in a semi-infinite body. *Communications in Numerical Methods in Engineering*, In Press, Accepted Manuscript, 2009.

Fachinotti V. and Cardona A. Constitutive models of steel under continuous casting conditions. *J. Materials Processing Technology*, 135:30–43, 2003.

Fachinotti V., Cardona A., and Huespe A. A fast convergent and accurate temperature model for phase-change heat conduction. *Int. J. Numer. Meth. Engng.*, 44:1863–1884, 1999a.

Fachinotti V., Cardona A., and Huespe A. Numerical simulation of conduction-advection problems with phase change. *Latin Am. Applied Research*, 31:31–36, 2001.

Fachinotti V.D. *Modelado Numérico de Fenómenos Termomecánicos en la Solidificación y Enfriamiento de Aceros Obtenidos por Colada Continua*. Ph.D. thesis, Facultad de Ingeniería y Ciencias Hídricas, Universidad Nacional de Litoral, Santa Fe, Argentina, 2001.

Fachinotti V.D., Cardona A., and Huespe A.E. A fast convergent and accurate temperature model for phase-change heat conduction. *Int. J. Numer. Methods Engrg.*, 44:1863–1884, 1999b.

Goldak J., Chakravarti A., and Bibby M. A new finite element model for welding heat sources. *Metallurgical Transactions B*, 15:299–305, 1984.

Huespe A., Cardona A., and Fachinotti V. Thermomechanical model of a continuous casting process. *Comput. Methods Appl. Mech. Engrg.*, 182:439–455, 2000.

Lindgren L.E. Finite element modeling and simulation of welding. part 2: Improved material modeling. *J. Thermal Stresses*, 24(3):195–231, 2001.

Nakagawa T., Umeda T., Murata J., Kamimura Y., and Niwa N. Deformation behavior during solification of steels. *ISIJ Int.*, 35(6):723–729, 1995.

Nami M., Kadivar M., and Jafarpur K. Three-dimensional thermal response of thick plate weldments: effect of layer-wise and piece-wise welding. *Modelling Simul. Mater. Sci. Eng.*, 12:731–743, 2004.

Özisik M. and Uzzell J. Exact solution for freezing in cylindrical symmetry with extended freezing temperature range. *Journal of Heat Transfer*, 101:331–334, 1979.

Simo J. and Hughes T. *Computational Inelasticity*. Springer-Verlag, New York, 1998.

Thomas B.G. and Parkman J.T. Simulation of thermal mechanical behavior during initial solidification. pages 2279–2285. 1997.

Weiner J. and Boley B. Elasto-plastic thermal stresses in a solidifying body. *J. Mech. Phys. Solids*, 11:145–154, 1963.

Yaghi A. and Becker A. State of the art review - weld simulation using finite element methods. Technical Report, University of Nottingham, UK, 2004.